9TH INTERNATIONAL SYMPOSIUM ON PARTICLE IMAGE VELOCIMETRY – PIV'11
Kobe, Japan, July 21-23, 2011

Holographic Correlation Velocimetry

Simon P. A. Higgins[1], Chaminda R. Samarage[1], David M. Paganin[2], Andreas Fouras[1]

[1]Division of Biological Engineering, Monash University,
Wellington Road, Clayton, Victoria 3800, Australia
andreas.fouras@monash.edu

[2]School of Physics, Monash University,
Wellington Road, Clayton, Victoria 3800, Australia

ABSTRACT

We describe a method for measuring three dimensional (3D) velocity fields of a fluid at high speed, by combining a correlation-based approach with in-line holography. While this method utilizes tracer particles contained within the flow, our method does not require the reconstruction of individual particle images. The direct flow reconstruction approach developed here, allows for measurements at seeding densities in excess of the allowable levels for techniques based on particle reconstruction. We outline the theory behind our method, which we term Holographic Correlation Velocimetry (HCV), subsequently applying it to both synthetic and laboratory data. Moreover, because the system is based on in-line holography, it is very efficient with regard to the use of light, as it does not rely on side scattering. This efficiency could be utilized to create a very high quality system at a modest cost. Alternatively, this efficiency makes the system appropriate for high-speed flows and low exposure times, which is essential for imaging dynamic systems.

1. INTRODUCTION

1.1 Particle Image Velocimetry (PIV)

There are many qualitative means for investigating fluid flow, including flow visualization methods using smoke, dye, or hydrogen bubbles [16]. To obtain a comprehensive, quantitative understanding of these flows, more sophisticated methods are required. Of these quantitative measurement techniques, the leading three are Hot-wire Anemometry (HWA) [8], Laser Doppler Anemometry (LDA) [25], and Particle Image Velocimetry (PIV) [1]. LDA and HWA are methods that measure discrete points in the fluid volume and may be used in an array or scanned through the flow to record data from throughout the flow volume. This can be a time consuming process and analyzing the discrete data stream from the flow volume may be difficult.

PIV is a full field, image based and therefore non-intrusive flow measurement technique that has been gaining popularity over the last two decades [2]. Tracer particles are introduced into the flow, and the region of interest is illuminated using a bright laser source (typically a pulsed Nd:YAG laser). Figure 1 shows a typical PIV setup. Assuming that the particles faithfully follow the flow, consecutive images of the illuminated region are captured using a high-speed digital camera. The images are discretized digitally into sub-regions and a cross-correlation analysis is performed in each sub-region [28]. The cross-correlation is representative of the probability distribution for the displacement of the underlying particle images in a sub-region, and the maximum signal is the most probable displacement between image frames. Since the time between image frames is known, the velocity of the flow captured in the region can be determined. Processing each of the discretized sub-regions results in a detailed velocity field of the flow. In many cases, it is enough to collect this data from a single plane in the flow. In this traditional form, the method provides no out-of-plane flow information. The most common solution to overcome this is stereoscopic PIV [4, 11, 13]; with two cameras the local out-of-plane velocity may be calculated. A number of fully 3D PIV variants have been developed [5] and are briefly described below.

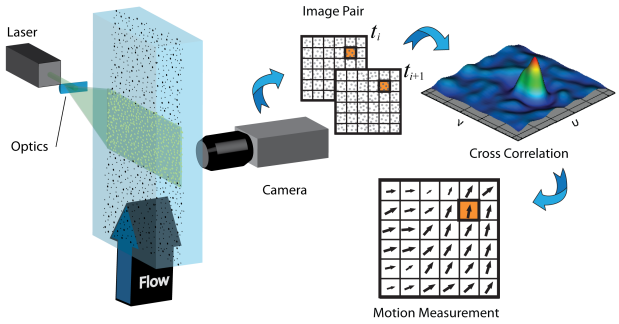

Figure 1. Schematic of conventional 2D PIV. A laser sheet illuminates tracer particles carried by the fluid flow, yielding image sequences captured with a digital camera. The images are discretized into sub-regions and the correlation between subsequent image sub-regions produces a vector of the local particle motion. From this correlation analysis, the fluid motion can be inferred.

1.2 Holographic PIV

Holographic PIV (HPIV) advanced the methods of recording a 3D instantaneous flow field in experimental measurements of fluid flow [6, 15]. HPIV started with film based holography, which involves using a reference beam to project the hologram, followed by a 2D plane detector being moved through the projected hologram to record the particle image field. Meng *et al.* looked at the use of film holography and the emergence of direct Digital HPIV [18]. But in either case, a method to extract velocity data from holographic images is required. This is commonly conducted using two methods, 3D PIV and Particle Tracking Velocimetry (PTV), both of which require reconstruction of the particle images before any inter-frame analysis can be performed [23]. We briefly review each method, in the following two sub-sections.

1.2.1 3D PIV

2D PIV techniques can be readily implemented and adapted for 3D particle fields [19]. In essence, this involves calculation of a spatial 3D cross-correlation using temporally adjacent images, the maximum value of which represents the most common displacement within the 3D sub-region. This requires a sufficiently high accuracy in reconstruction of the particles. Obtaining the precise position of small particles in space, from a hologram, is limited by the depth of focus problem [20]. To overcome this, multi angle in-line holography [23] and multiply off axis holography [21] or a combination of both [6] have been used. However these systems are complex and

require accurate calibration and alignment of cameras for corresponding voxel positions [23] and very few groups worldwide utilize this approach.

1.2.2 3D Particle Tracking Velocimetry (PTV)
PTV also requires many individual particles to be reconstructed in space and identified in successive frames in order to track them through the flow. Frequently the seeding density needs to be drastically reduced in order to obtain images in which particles can be unambiguously identified in 3D space. This is because if particles move in front of or behind one another the tracking position will be lost. With low particle seeding density, collecting data at all regions of the measurement volume is time consuming. To improve this, Pu and Meng [21], derived a Concise Cross Correlation and particle pairing algorithm [20]. This work used a 3D PIV correlation in discretized volumes, subsequently applying particle tracking to particles within the said volume. The dominant source of error in these techniques is the accurate reconstruction of the particles in the 3D volume.

1.3 Holographic Correlation Velocimetry (HCV)
In this paper, an alternative approach for volumetric flow measurement is proposed. The proposed holographic technique utilizes a correlation-based analysis to produce the full 3D velocity field without the need for reconstructing any seeding-particle image. This method reduces processing for digital inline holographic reconstruction and 3D velocity mapping. The method does not use complicated calibration and can be performed with relatively low powered lasers. This technique has been titled Holographic Correlation Velocimetry (HCV).

2. DESCRIPTION OF HOLOGRAPHIC CORRELATION VELOCIMETRY

2.1 Encoding of Depth Information
Unlike PTV, the technique described in this paper is based on a cross-correlation analysis. Fouras *et al.* [14] developed a technique by which the depth information in a seeded flow was encoded by the point spread function of the lens used to form the images. In HCV, the depth information of the particles is encoded by the particle diffraction pattern that varies with the propagation distance, z. Figure 2 illustrates the concept of how the depth information is encoded. When the Fresnel number, $N_F=a^2/(\lambda z)$, is much less than unity – where a, is the seed-particle diameter and λ, is the radiation wavelength – Fraunhofer diffraction is applicable [7]. Given the scaling of the Fraunhofer pattern in direct proportion to z, similar sized particles at different distances from the image plane will yield diffraction patterns that are transversely scaled with respect to one another. Hence the change in the appearance of a given particle's diffraction pattern is principally due to its distance from the image plane.

This method utilizes the first Born approximation that states that the optical energy density contained in the scattered beam, Ψ_s, must be significantly less than that which is contained in the unscattered beam, Ψ_o, at each point within the scattering volume: [7]

$$|\psi_s| = |\psi_o|. \quad (1)$$

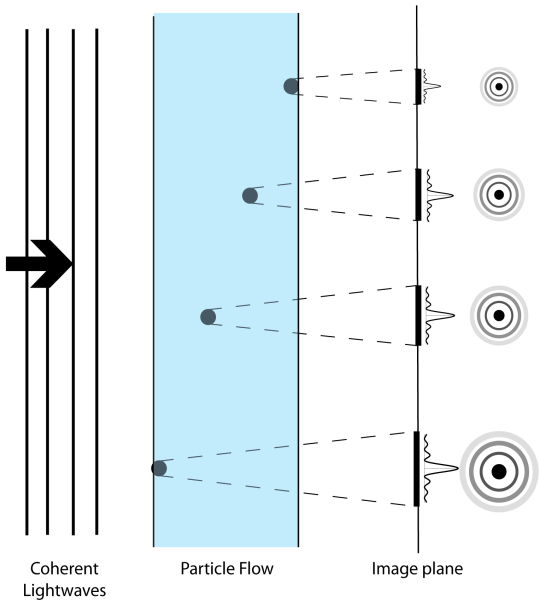

Figure 2. As coherent light is scattered by particles they produce a diffraction image of the particle, which in the far field will transversely scale with distance from the image plane. Particles nearer to the image plane produce diffraction rings that are transversely compressed relative to the rings produced by particles further from the image plane. The measured volume gives a speckle pattern comprised of all the overlapping rings.

For this to hold, the ratio of total illuminated area of particles to the total area must be significantly less than 1:

$$\frac{N\pi r^2}{A} \ll 1, \quad (2)$$

where N is the number of particles, r is the radius of the particles and A is the total area. Since the number of particles, N, is given by the ratio of the volume of the particles to the volume of a single particle, we obtain the following inequality as a sufficient condition for the applicability of the first Born approximation:

$$\frac{T\phi}{r} \ll \frac{4}{3} \quad (3)$$

where T and ϕ represent the sample thickness and particle volume fraction respectively. For our situation we have a T =10mm, $\phi = 2.9\times10^{-5}$ and r = 5μm; this yields $T\phi/r = 0.058$, which clearly satisfies inequality (3). Hence the first Born approximation is applicable to our analysis.

Figure 3 shows two inline holograms, H_1 and H_2, of a volume at two closely-spaced successive time points, t_1 and t_2 over a range of z. P_i and Q_i represent sub images of H_1 and H_2 such as would be formed if only the particles within the slab z_i were imaged. Under the first Born approximation [9], and ignoring interference between adjacent particles as irrelevant to our correlation-based analysis, H_1 is the sum of all P_i and H_2 is the sum of all Q_i. The current method is based on the key assumption that the cross-correlation of the full projected images, is equal to the sum of the cross-correlations of sub image pairs.

This proposition assumes that the thickness of each individual slice in z, is greater than the particle diameter, and that there is

no inter-particle correlation between tracer particles in distinct slabs. A basic proof of this can be formulated as follows[1]:

$$\sum_{i=1}^{N}\left(P_i * Q_i\right) = \sum_{i=1}^{N}\sum_{j=1}^{N}\left(P_i * Q_j\right). \quad (4)$$

Since there is no inter-particle correlation between adjacent slabs,

$$P_i * Q_j = 0 \quad \text{for i} \neq \text{j}, \quad (5)$$

hence,

$$\mathrm{H}_1 * \mathrm{H}_2 = \sum_{i=1}^{N}(P_i * Q_i). \quad (6)$$

A limitation with current techniques is the particle concentration, whereby high levels of particle seeding can lead to challenges in reconstructing the particle image positions. However, with HCV, a higher level of seeding aids in improving the quality of the cross-correlation that has the depth information readily encoded.

1. Here, an asterisk (*) denotes a two-dimensional discrete convolution.

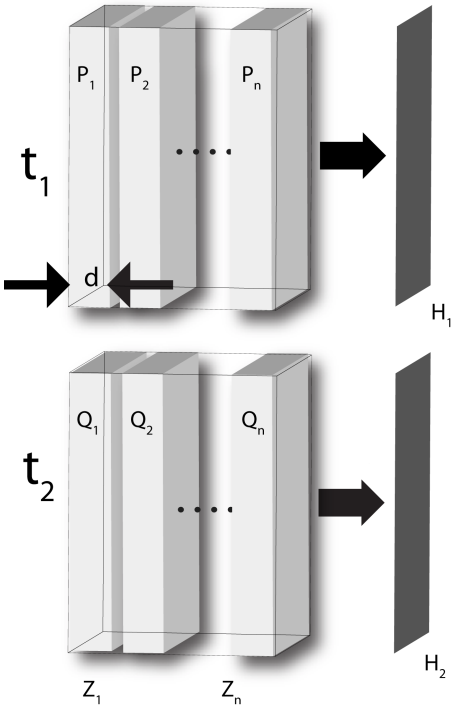

Figure 3. Two holographic images H_1 and H_2, at two successive time points, t_1 and t_2 for a range of z. P_i represents the inline hologram due to slice z_i at $t=t_1$, and Q_i is similarly defined at $t=t_2$. Under the assumption of weak scattering by each slab, and neglecting both interference between adjacent particles and an irrelevant additive constant, $H_1=\sum_i P_i$ and $H_2=\sum_i Q_i$.

2.2 Decoding of Depth Information

Under the above model for holographically encoding the depth information in the seeded flow, we can formulate an approach by which over a specified depth, we may model a full cross-correlation function for the entire volume.

As customary in PIV, the projected holographic images are discretized into sub-regions. Within each sub-region (which is 2D in the projected image domain), an analytical model of the flow is developed in which the velocity of the flow is specified as a function of z. In this case we have chosen to use an Akima spline [3] as this model. From the known velocity field, the probability distribution function (PDF) is readily calculated.

It is well known that the cross-correlation is the convolution of the auto correlation (AC) and the probability distribution function for the displacement [12, 14, 10]:

$$CC = AC * PDF \quad (7)$$

Since the auto correlation varies with z, we invoke equation (7) to give:

$$CC = \sum_{z=1}^{n}\left(AC(z) * PDF(z)\right) \quad (8)$$

Since AC(z) can be evaluated analytically, or, in the laboratory by imaging a monolayer of particles, at several z locations; we have a methodology for constructing the cross-correlation map for any given flow field.

Based on this model, we can iteratively reconstruct the 3D velocity field by minimizing the error between the full cross-correlation map from the flow model described above, and the 2D cross-correlation map, obtained for the same sampling region from standard PIV. We use a Levenberg-Marquardt [19, 20] non-linear least-squares solver to perform the error minimization. Figure 4. is an illustration of this iterative process to which is implemented in HCV.

Once the in-plane flow has been reconstructed, the out-of-plane flow can be calculated with the assumption that the fluid is incompressible, the volume is fixed, and the flow obeys the law of continuity.

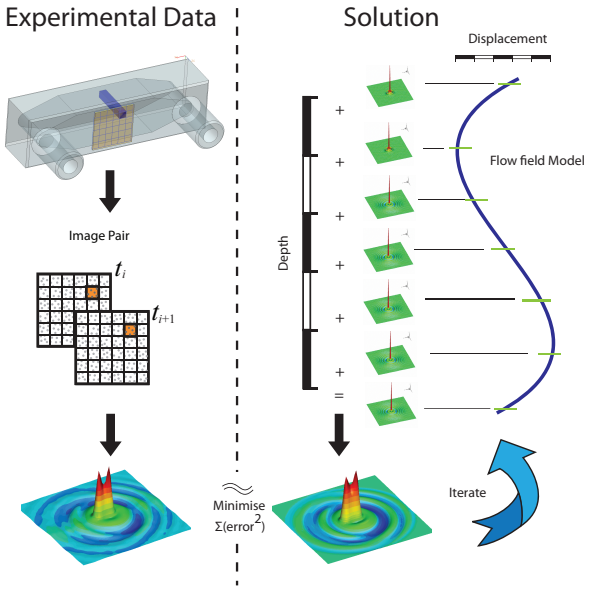

Figure 4. Graphical representation of the Holographic Correlation Velocimetry (HCV) algorithm. The algorithm solves for the 3-dimensional flow field by iteratively reconstructing the volumetric cross-correlation until the residual of the reconstructed cross-correlation and the measured cross-correlation reaches an acceptable level.

3. MODELING

3.1 Synthetic Image Generation

To validate the method described in section 2.2, computer modeling was conducted via generation of synthetic holographic images of particles. These particles are displaced by a known velocity function between successive images. This simulates a flow field of particles in a laboratory fluid flow. There is complete control over the refractive indices and the noise component to the images. The synthetic images are

generated with equations from Widjaja & Soontaranon [27] and Tyler & Thompson [26] that are used for holographic particle size analysis and utilize the first Born approximation insofar as they neglect multiple scattering between distinct particles. The parameters for these synthetic images were: 532nm illumination, 105mm objective lens, 5000 particles of 10μm diameter particles per image, and an image of 1024×1024 pixels with pixel size 7.4μm. These images are discretized into sub-regions and cross-correlations are generated between successive image pairs. These correlation maps are then decoded in order to determine the velocity through the depth of the discretized sub-regions.

Figure 5 contains synthetically generated images of particle fields (a,b) and the averaged spatial auto-correlation of their corresponding inline holograms (c,d). The data in a and c represents particles imaged at the contact plane (i.e. z=0), while the particles in b and d are at 20mm propagation distance. Fig. 6 shows two example cross-correlation functions of the inline holograms of single-layer particle fields at a small propagation distance and medium propagation distance.

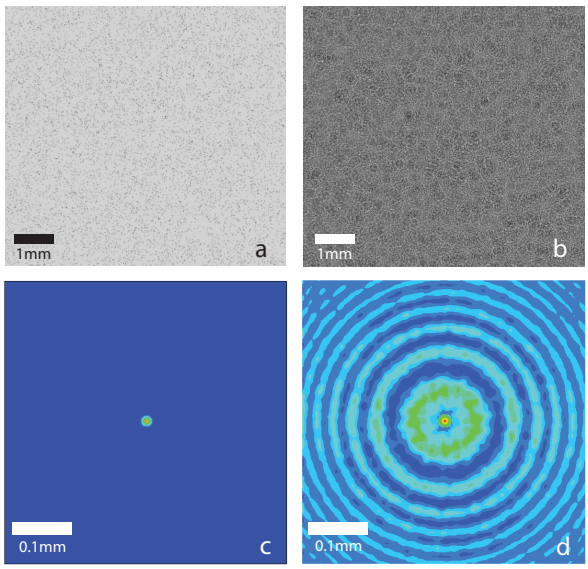

Figure 5. Synthetic image data of particle fields (a,b) and the averaged spatial auto-correlation of the corresponding inline holograms (c,d). The data in a and c represents particles imaged at contact (i.e. z=0), while the particles in b and d are at 20mm propagation (λ=532nm).

3.2 Results of Synthetic Experiments

The results for the synthetic modeling shown in this paper are generated by representing the variation of velocity field in the depth direction with a cubic polynomial. Figure 7 shows the flow input function with 100 data points for the solution fitting function. These data points are the velocity at each of these channel depth locations. Figure 8 gives a side-by-side comparison of a single correlation function from the input synthetic data field and from the output model solution. It can be seen clearly that the model adequately approximates the synthetic data. This flow has been chosen due to its complexity with particles in different depth planes moving in opposite directions, thereby stretching and spreading the correlation map. Nevertheless, the algorithm is able to fit the calibration maps to the data and solve for the correct flow. In the simple parabolic case, there may be several similar solutions negatively affecting the results. But in these cases, this is compensated for by the capacity to supply a good initial approximation for the 3D HCV from 2D PIV analysis of the image sets. With promising results in the synthetic case studies experimental work was conducted and investigated, as reported in section 4.

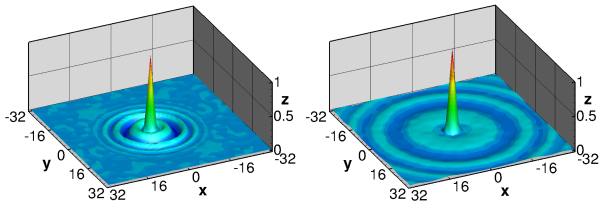

Figure 6. Two, 64×64 pixel normalized, auto-correlation maps from synthetic holographic calibration images of particles having a nominal diameter of 10μm in a single plane. The left frame corresponds to a propagation distance of 3mm and the right is at 14mm. At 0mm there are no rings visible in the auto correlation. The position and subsequent summation of this calibration map is used to replicate the data correlation maps yielding the velocity direction and intensity at different depths in the flow.

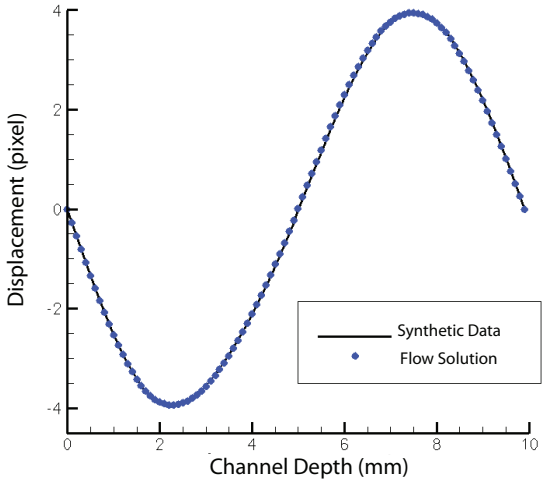

Figure 7. A plot of synthetic flow measurement experiments. The synthetic data (the simulated shear flow between two infinite plates) is shown as a continuous line, with the recovered function indicated by dots. The solution resolved both positive and negative velocity directions from individual cross-correlation maps as illustrated in Figure 8. The normalized RMS difference between the synthetic data and the flow solution is 0.72%.

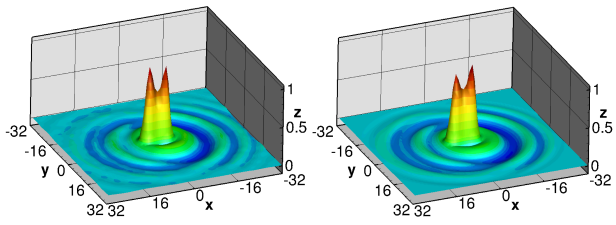

Figure 8. Two, 64×64 pixel normalized, cross-correlation maps. The left shows the cross-correlation of two synthetic image sub-regions, while the right shows the cross-correlation from the combination of calibration maps with the flow model solution.

4. LABORATORY EXPERIMENTS

4.1 Set up

A Nd:YAG laser (Darwin λ=532nm) running at 30kHz was used to generate collimated inline illumination. This was projected through the Flow Cell (Hellma®137-QS, 10mm) filled with glycerin seeded with glass particles having a nominal diameter of 10μm. The particles have a size distribution with 10% having a diameter less than 3.45μm, 50% less than 9.1μm and 90% less than 20.31μm. The holograms of these particles were imaged with a CMOS camera (IDT Y4) with a 200mm lens (Nikon) set with its focal plane 5mm from the front of the flow cell to allow optimal propagation for the near particles compared to the particles on the far side of the channel. Each image records a volume containing on the order of 2.3×10^4 particles, which satisfies the first Born approximation as discussed in section 2.1. The flow of particles was maintained with a peristaltic pump through a muffler (to remove pulsatility) into an open reservoir as illustrated in Figure 9. The Reynolds number represents the ratio of momentum to viscous forces and is given by $Re=(\rho uD)/\nu$, where ρ is the density, u is a representative velocity, D is the representative length scale and ν is the dynamic viscosity. The Reynolds number of this flow based on the inlet diameter of 2mm is 1.77. The cross section of the channel is 9mm×10mm. The exposure time for the CMOS chip was 762μs at a 50Hz frame rate. As the system is based on in-line holography, it is very efficient with regard to the use of light, as it does not rely on side scattering. Most other volumetric measuring systems rely on off-axis or side-scattered light, which requires high power lasers. This efficiency makes the system appropriate for high-speed flows and lower exposure times. Once the images are captured the analysis is completed on a PC. The calibration images that are used for the algorithm to solve the model for the flow were acquired at 100 depth positions.

4.2 Data Treatment

Images are first filtered to remove stationary artifacts. This background subtraction was performed using the local temporal average of the image sequence. The images are discretized into sub-regions and the cross-correlation map between images frames is computed for each discrete sub-region. These correlation maps have been time averaged as described by Meinhart *et al*. [17]. It has been shown that averaging the correlation maps results in an improved signal to noise ratio. This has been recently shown to increase the effective seeding density of the data set [22]. This effective increase in seeding density in the correlation space does not affect the validity of the first Born approximation in our analysis. The image sub-regions of 64×64 pixels were evaluated with a spacing of 16×16 pixels in x and y. This achieves an overlap of 75%, which has been shown to be optimal [24]. These correlations are produced using a zero padded fast Fourier transform (FFT) function to prevent any wrapping effects over the 64 pixels sub-region of the diffraction fringes from the particles at long propagation distances.

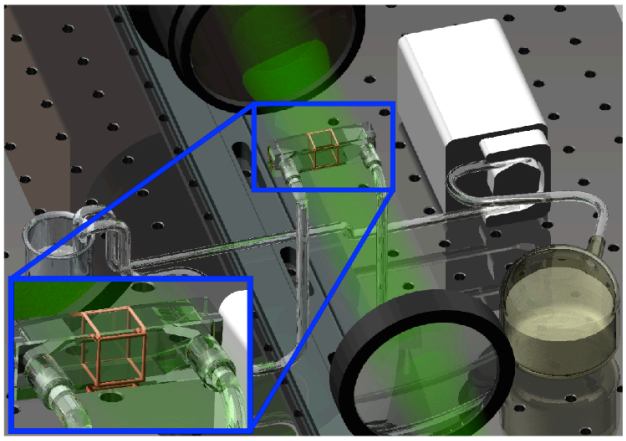

Figure 9. Experimental setup for Holographic Correlation Velocimetry. Shown are the laser, optics, camera, lens, and flow cell attached to the peristaltic pump. A Nd:YAG laser (Darwin 532nm) running at 40kHz was used to generate the inline illumination. This was projected through the Flow Cell (Hellma® 137-QS, 10mm), which was filled with glycerin mixed with 10μm glass particles. This seeded flow was imaged with a CMOS camera (IDT Y4) at 1000fps with a 200mm macro lens (Nikon) set with the focal plane 5mm from the front of the flow cell for optimized propagation. This flow was maintained with a peristaltic pump through a muffler to remove pulsatility and into an open reservoir. The inset shows the region that is being measured with HCV.

For our experimental work, we found that utilizing experimental calibration images introduced errors to the solution. This error was removed by utilizing synthetic, noise free calibration images, and was implemented in the analysis throughout the rest of this paper.

The 2D PIV results that reveal the modal velocity of the flow field are used to give the first approximation of the solution to the least-squares solver. This allows the algorithm to rapidly converge at an accurate local minimum in what is a very large parameter space.

4.3 Results of Experimental Data

Figure 10 shows a single slice of the flow in the channel displayed for orientation and context. It is necessary to note that the highest flow rate is toward the back wall on the opposite side of the from the inlet and outlet ports. The plane shown is towards the inlet port that is in effect acting like a jet into a volume. With this in mind it can be understood that because the fluid has momentum as it exits the jet it will be carried to the back wall and then through the channel. Figure 11 shows contours for the magnitude of velocity in a single slice of the reconstructed flow field. On the z axis zero is the back wall and we see that the flow is predominantly faster in the lower half of the channel. The flow is extremely symmetrical which is to be expected from the inlet port being on the centerline of the channel. The corners of the channel clearly illustrate very slow flow occurring here. Again this is expected in the area where the two walls meet and there is a high drag on the fluid.

To best illustrate that the full 3D volume of the flowing fluid is reconstructed, Figure 12 shows the vectors of over 400,000 points. The spacing between these points is 0.2mm in the x and y plane and 0.1mm in the z or depth direction. The vector color is velocity magnitude and there is a single slice of the velocity contour levels.

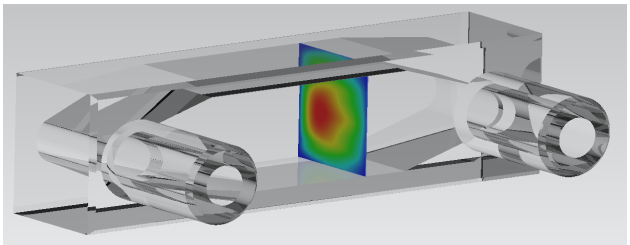

Figure 10. An illustration of the flow channel with the velocity field in-situ (shown in more detail in Figure 11). The inlet and outlet are shown on the near surface of the (Hellma®) manufactured from fused Quartz (SUPRASIL®). The square cross section of the channel is 9mm×10mm ±0.01mm.

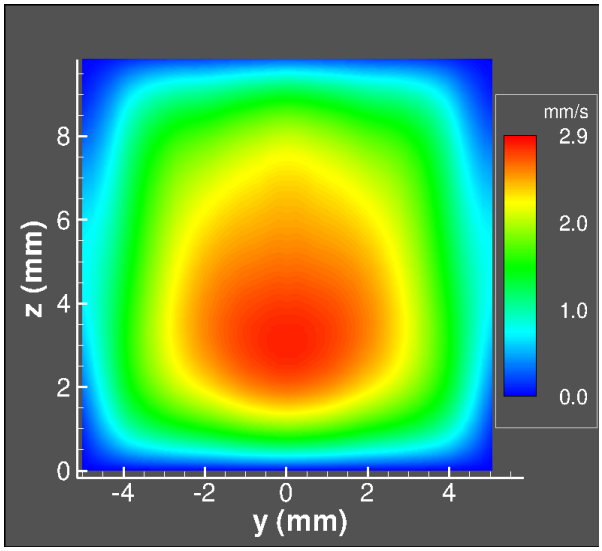

Figure 11. Reconstruction of the velocity magnitude of a single slice of the measured flow within the 9mm×10mm flow cell. As the flow enters from the top of the cell (*z*=10mm) in a jet like fashion, the momentum carries fluid towards the bottom of the cell (*z*=0mm). The peak velocity magnitude is therefore not on the centerline, but closer to the bottom. The flow is symmetric about the centerline at *y*=0mm, as expected with the cell geometry.

5. CONCLUSION

In this paper an improved approach for volumetric flow measurement has been developed, in which the correlations of inline holograms can be successfully used to generate a full 3D velocity field of a seeded fluid. It has been shown that these correlations have encoded depth information providing the velocity at different depths within the fluid. This method allows flow reconstruction without the need to reconstruct the individual particles within the 3D volume. Holographic Correlation Velocimetry (HCV) allows for the direct measurement of the velocity field at all depth locations through the use of the volumetric correlation function. Not reconstructing the 3D particle field offers advantages over other HPIV and Digital HPIV systems by directly producing velocity data from 2D images. Since the system does not rely on side scattering, the system makes very efficient use of available light. This efficiency could be utilized to create a high quality system at a modest cost. Alternatively, this efficiency allows low exposure times and the dynamic measurement of high speed flows.

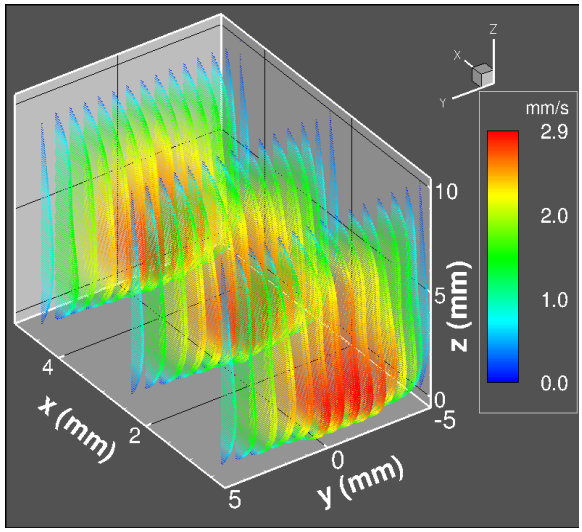

Figure 12. Reconstructed 3D vector field of the fluid flow within the measurement volume. There are approximately 400,000 vectors (colored with velocity magnitude) in the solution. For the sake of clarity, vector resolution has been decreased in *x* and *y*-axes.

ACKNOWLEDGMENTS

The authors would like to thank Stephen Dubsky for the insightful discussions in developing HCV. The authors acknowledge funding from the Australian Research Council, via the Discovery Projects scheme under DP0987643 and DP0773650.

REFERENCES

[1] Adrian R. J., (1991) Particle-imaging techniques for experimental fluid-mechanics, *Annu. Rev. Fluid Mech.,* **23,** 261-304

[2] Adrian R. J, (2005) Twenty years of particle image velocimetry, *Exp. Fluids,* **39,** 159-69

[3] Akima H., (1970) A new method of interpolation and smooth curve fitting based on local procedures, *J. Acm.* **17,** 589-602

[4] Arroyo M. P. & Greated C. A., (1991) Stereoscopic particle image velocimetry, *Meas. Sci. Technol.,* **2,** 1181-6

[5] Arroyo M. P. & Hinsch K. D., (2008) Recent developments of PIV towards 3D measurements, *Top Appl. Phys.,* **112,** 127-54

[6] Barnhart D. H., Adrian R. J. & Papen G. C., (1994) Phase-conjugate holographic system for high-resolution particle-image velocimetry, *Appl. Optics,* **33,** 7159-70

[7] Born M. & Wolf E., (1999) *Principles of Optics, seventh (expanded edition),* Cambridge University Press, Cambridge

[8] Comte-Bellot G., (1976) Hot-wire anemometry, *Annu. Rev. Fluid Mech.,* **8,** 209-31

[9] Cowley J. M., (1995) *Diffraction physics,* Elsevier, Amsterdam

[10] Dubsky S., Jamison R. A., Irvine S. C., Siu K. K. W., Hourigan K. & Fouras A., (2010) Computed tomographic x-ray velocimetry, *Appl. Phys. Lett.,* **96,** 023702

[11] Fouras A., Dusting J. & Hourigan K., (2007) A simple calibration technique for stereoscopic particle image velocimetry, *Exp. Fluids,* **42,** 799-810

[12] Fouras A., Dusting J., Lewis R. & Hourigan K., (2007) Three-dimensional synchrotron x-ray particle image velocimetry, *J. Appl. Phys.,* **102,** 064916
[13] Fouras A., Lo Jacono D. & Hourigan K., (2008) Target-free Stereo PIV: a novel technique with inherent error estimation and improved accuracy, *Exp Fluids,* **44,** 317-29
[14] Fouras A., Lo Jacono D., Nguyen C. V. & Hourigan K. (2009) Volumetric correlation PIV: a new technique for 3D velocity vector field measurement, *Exp Fluids* **47,** 569-77
[15] Hinsch K. D. (2002) Holographic particle image velocimetry, *Meas Sci Technol* **13,** R61-R72
[16] Mahir N. & Rockwell D. (1996) Vortex formation from a forced system of two cylinders.1. Tandem arrangement, *J Fluid Struct* **10,** 473-89
[17] Meinhart C. D., Wereley S. T. & Santiago J. G. (2000) A PIV algorithm for estimating time-averaged velocity fields, *J Fluid Eng-T Asme* **122,** 285-9
[18] Meng H., Pan G., Pu Y. & Woodward S. H. (2004) Holographic particle image velocimetry: from film to digital recording, *Meas Sci Technol* **15,** 673-85
[19] Ooms T., Koek W. & Westerweel J. (2008) Digital holographic particle image velocimetry: eliminating a sign-ambiguity error and a bias error from the measured particle field displacement, *Meas Sci Technol* **19,** 074003
[20] Pan G. & Meng H. (2001) Digital in-line holographic PIV for 3D particulate flow diagnostics. In: *PIV '01: 4th International Symposium on Particle Image Velocimetry* (Göttingen, Germany pp 17-9
[21] Pu Y. & Meng H. (2000) An advanced off-axis holographic particle image velocimetry (HPIV) system, *Exp Fluids* **29,** 184-97
[22] Samarage C. R., Carberry J., Hourigan K. & Fouras A. (2011) Optimisation of temporal averaging processes, *Exp Fluids - in press,* DOI: 10.1007/s00348-011-1080-8
[23] Soria J. & Atkinson C. (2008) Towards 3C-3D digital holographic fluid velocity vector field measurement - tomographic digital holographic PIV (Tomo-HPIV), *Meas Sci Technol* **19,** 12
[24] Theunissen R., Scarano F. & Riethmuller M. L. (2007) An adaptive sampling and windowing interrogation method in PIV, *Meas Sci Technol* **18,** 275-87
[25] Tropea C. (1995) Laser-doppler anemometry - recent developments and future challenges, *Meas Sci Technol* **6,** 605-19
[26] Tyler G. A. & Thompson B. J. (1976) Fraunhofer holography applied to particle-size analysis - reassessment, *Opt Acta* **23,** 685-700
[27] Widjaja J. & Soontaranon S. (2009) All wavelet analysis of in-line particle holograms, *Opt Laser Eng* **47,** 1325-33
[28] Willert C. E. & Gharib M. (1991) Digital particle image velocimetry, *Exp Fluids* **10,** 181-93